Modular Spectrum Utilization for Next-Generation Fixed Transmission Networks

Invited Paper

Jordan Naterer, Elena Dobre, Ayman Mostafa, Lutz Lampe
University of British Columbia, BC, Canada

***Abstract*—Wireless transmission signals need to comply with spectrum masks usually defined in standards for the associated wireless systems and frequency bands. A spectrum mask typically consists of the main spectrum part intended for the communication signal and spectrum skirts to regulate spurious emissions and permit adjacent channel usage. Interestingly, the spectrum skirts can also be used to notably improve the data rate if the signal-to-noise ratio in the transmission link is fairly high and adjacent frequency channels are unused. These two conditions are met with high probability in fixed microwave transmission links. For this reason, in this paper, we propose two communication methods that take advantage of these unused sidebands. The methods are modular in that a secondary signal which occupies the skirts of the spectrum mask is added to the main data signal. The first method uses superposition and adds a secondary low-power signal to the primary high-power signal with spectral overlap. The second method uses a multi-carrier transmission approach with custom pulse shapes for the sidebands to fit under the spectrum mask. We compare the performance of these methods in terms of achievable rate with that for conventional microwave transmission not using spectrum skirts under realistic conditions. In particular, to highlight the benefits of our approach, we consider practically relevant levels of local oscillator phase noise, which is the limiting factor when selecting the order of modulation used in microwave systems.**

***Index Terms*—Microwave transmission systems, spectrum skirts, superposition transmission, multi-carrier transmission.**

I. Introduction

The insistent rise of mobile data service demands continuously increases the data requirements for global communication networks. Furthermore, the fifth generation of wireless communications places greater emphasis on data requirements for use cases such as ultra-reliable low-latency communications and massive machine type communications in Internet-of-Things devices. Gradually over the years, the bottleneck of radio access network capacity has shifted from the radio interface to the backhaul network.

Backhaul links are commonly established either by high capacity optical fibre lines, or low cost fixed microwave wireless links. While optical fibre can achieve significantly higher data rates and larger capacities, the high cost of deployment and the geographical installation constraints are restrictive. On the other hand, microwave links can be quickly deployed and require a lower capital expenditure compared to fibre. Also, microwave transmission is the preferred medium for the backhaul of the next generation of cellular networks in cases where optical fibre links cannot be deployed [1]. However, microwave transmission requires spectrum leasing, which raises the operating expense of the network.

Frequency spectrum regulations in microwave transmission bands ensure that systems operating in adjacent frequency channels do not interfere with one another. However, it is observed in many higher frequency microwave links that channels which are used in the same transmission hop have unoccupied neighbouring channel slots. For example, our analysis of the latest spectrum allocation database in the 18 GHz band in the USA [2] showed that only 1.2% of fixed point-to-point transmit channels have active neighbours. Similar results have been found for microwave bands in Canada and the UK for example [3, Fig. 1]. Hence, from the perspective of a communication link there is no interference from a neighbouring channel in the spectrum skirt regions. At the same time, the signal-to-noise ratio (SNR) levels experienced by fixed microwave links are, for the majority of time, sufficiently high to support reliable communication in spectrum skirts. For example, fixed microwave links experience SNRs of around 45-50 dB and higher for 99% of the time in a year [4].

We propose using the spectrum skirts for data transmission to increase the data rate achievable within a single microwave transmission channel without additional costs for licenses. In previous work [3], some of us have developed single-carrier pulse-shaped transmission to leverage this opportunity. In this paper, we introduce two alternative transmission methods that, different from [3], consist of the conventional microwave transmission signal and additional signal components (or data streams) that can be placed in spectrum skirts. Compared to the solution in [3], the new methods have the advantage that the use of spectrum skirts can be turned on or off by adding additional data streams in a modular fashion. The proposed methods are complementary to other approaches for improving spectral efficiency such as dual-polarization or multiple antenna transmission.

The first new method, which we refer to as superposition transmission, overlaps the strong primary signal with a weak secondary signal whose power spectral density (PSD) extends

The co-authors dedicate this paper to the main contributor Jordan Naterer, who has been missing since October 2020. Our thoughts are with him.

This work was supported by the Natural Sciences and Engineering Research Council of Canada (NSERC) and Huawei Technologies Canada.

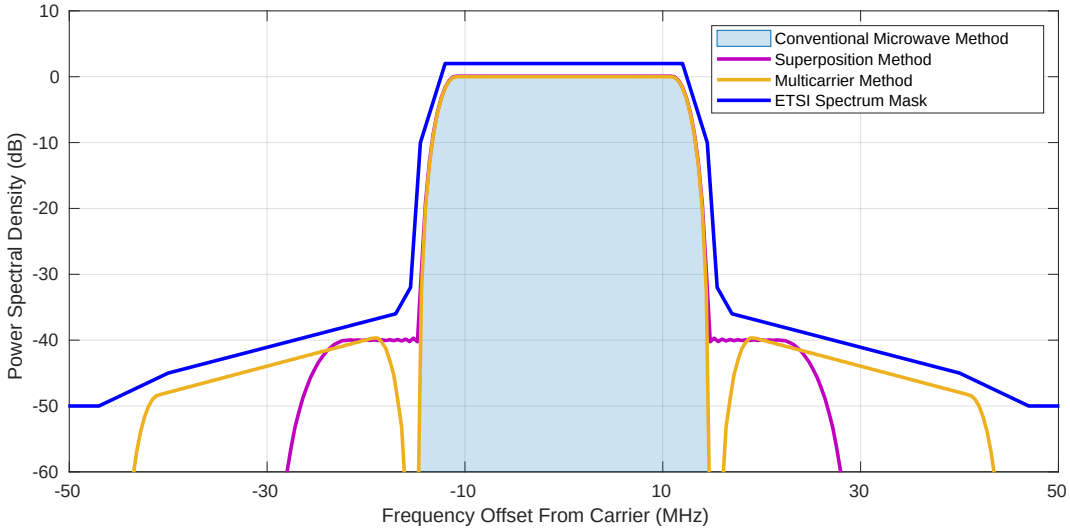

Fig. 1: Illustration of the use of spectrum skirts for a spectrum mask according to [5]. The conventional microwave system uses a root-raised cosine pulse, which can occupy a bandwidth of 29.4 MHz for the chosen emission mask. The power spectral densities for the superposition and multi-carrier transmission schemes show the use of spectrum skirts.

to the spectrum skirts. We present an interference cancellation method for the detection of these two signal streams. The second method uses a multi-carrier approach and adds two low-power sideband signals, which are orthogonal to the main signal. For the multi-carrier method, we apply the approach from [3] to design custom pulse shapes that fit under the spectrum mask to best exploit the available sidebands. In all cases, we consider transmission impairments such as a dispersive channel and local-oscillator phase noise, which are experienced by practical microwave links. It should be noted that phase noise is limiting the performance of microwave communication links operating at high SNRs. In particular, the maximum constellation size suitable for reliable communication is limited by phase noise impairments. Our numerical performance results show that both schemes offer data rate improvements on the order of 30% and 40% over conventional microwave transmission.

II. Transmission Schemes for Modular Spectrum Utilization

In this section, we introduce the two new methods which use the spectrum skirts. Figure 1 shows a spectrum mask for microwave transmission in the 17-30 GHz band according to [5, Table 3e] together with the PSDs for (i) a conventional microwave system employing a root-rased cosine (RRC) pulse shape, (ii) the superposition transmission method, and (iii) the multi-carrier transmission method. In the following we will provide the details for the latter two.

A. Superposition Transmission

The first spectrum utilization method overlaps two carrier signals at the transmitter and sequentially detects them at the receiver. The transmitter architecture in Fig. 2 (left subfigure) is similar to a standard microwave link, with a signal chain added to the primary stream before analog up-conversion and antenna transmission. The continuous-time representation of the superposition transmission signal is

$$s(t) = \sqrt{P_1}\sum_k I_1[k]p_1(t-kT_1)+\sqrt{P_2}\sum_k I_2[k]p_2(t-kT_2), \tag{1}$$

where $I_1[k]$ and $I_2[k]$ are the quadrature amplitude modulation (QAM) symbols of the primary and secondary data streams, respectively. The pulse shapes $p_1(t)$ and $p_2(t)$ represent the narrowband and wideband pulses used to shape our primary and secondary pulses, while T_1 and T_2 denote each stream's symbol interval. Furthermore, P_1 and P_2 are the powers for the two streams. The QAM orders of each stream may vary based on channel conditions.

Regarding pulse shapes, the superposition scheme allows the second stream to incorporate a larger bandwidth to effectively utilize the spectrum skirts. For example, the PSD for the combined RRC pulse shapes with Nyquist rates of 25.6 MHz and 51.2 MHz and a roll-off factor of 0.15 are displayed in Fig. 1. Transmitting the secondary stream at a symbol rate that is double the primary stream, i.e., $T_2 = T_1/2$, implies a 40 dB difference in transmit powers P_1 and P_2 to meet the spectral mask constraints.

The continuous-time representation of the received baseband signal is expressed as

$$r(t) = \mathrm{e}^{\mathrm{j}\phi_\mathrm{r}(t)}\int_{-\infty}^{\infty} s(\tau)\mathrm{e}^{\mathrm{j}\phi_\mathrm{t}(\tau)}h(t-\tau)d\tau + n(t), \tag{2}$$

where $h(t)$ denotes a multipath channel, usually modelled according to [6] for microwave links, and $n(t)$ denotes additive white Gaussian noise (AWGN). Furthermore, $\phi_\mathrm{t}(t)$ and $\phi_\mathrm{r}(t)$ represent the transmitter and receiver phase noise processes, respectively. The receiver architecture in Fig. 2 (right subfigure) is more complex than the transmitter, as it requires

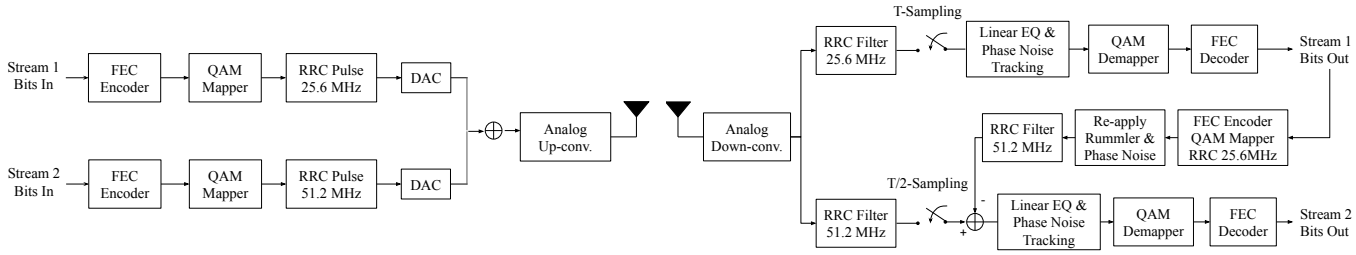

Fig. 2: Superposition transmission scheme architecture. The displayed baud-rate figures are example settings, applying the spectrum mask for the 17-30 GHz band according to [5, Table 3e] and being consistent with the PSD for superposition transmission shown in Fig. 1.

removal of the primary stream to detect the secondary stream. First, the received signal $r(t)$ is passed through two matched filters with bandwidths according to the transmitter pulse shapes for the two data streams. Figure 2 provides specific values for the pulse shapes and bandwidths considering the 17-30 GHz transmission band with the spectrum mask from [5, Table 3e]. Then, the primary data stream is detected by applying a linear equalizer to handle the distortion from the dispersive channel, a phase noise compensation method to eliminate phase noise, and demapping and forward-error correction (FEC) decoding. Once the primary stream has been decoded, it is re-encoded and estimations of the dispersive channel and channel phase noise samples are re-applied. This reconstruction is necessary to detect the secondary stream. In particular, after re-applying channel impairments, the first stream is subtracted from the received signal at a larger bandwidth, so that the secondary stream can be decoded with ideally no interference from the primary stream. The main bottleneck for this receiver architecture is the accuracy of reconstruction of the primary stream. While equalization and phase noise removal are important for the secondary stream operating at a lower signal power, the residual interference from the primary stream is the limiting factor when detecting the secondary stream due to the large power difference.

B. Multi-Carrier Transmission

The second spectrum utilization method transmits three pulses simultaneously while remaining orthogonal in the frequency domain. The two secondary pulses are sent adjacent to the primary pulse via an offset frequency and rely on well designed transmitter and receiver filters to neglect interference.

The transmitter architecture is shown in Fig. 3 (left subfigure). The continuous-time baseband representation of the multi-carrier signal is given by

$$s(t) = \sqrt{P_1}\sum_k I_1[k]p_1(t-kT) + \sqrt{P_2}\sum_k I_2[k]p_2(t-kT) + \sqrt{P_3}\sum_k I_3[k]p_3(t-kT), \tag{3}$$

where $I_1[k]$, $I_2[k]$, and $I_3[k]$ are the QAM symbols of the primary and two secondary streams and P_1, P_2, and P_3 are the respective signal powers. The pulse shapes $p_1(t)$, $p_2(t)$, and $p_3(t)$ represent the pulse shapes of the primary and two secondary streams transmitted at symbol interval T. The frequency offsets for the secondary streams are incorporated into each pulse shape.

Since the three pulses are orthogonal in the frequency domain, we have the ability to use custom pulse shapes to fill more of the spectrum mask for the side streams. We may formulate this objective as an optimization problem to match the spectrum mask as closely as possible. We consider a linear-phase discrete-time filter of length $2N+1$, and organize the real and imaginary parts of the filter coefficients in the vectors $\mathbf{p}_{\text{re}}$ and $\mathbf{p}_{\text{im}}$, respectively. Then, the discrete-time Fourier transform is given by

$$P(f) = \mathrm{e}^{-\mathrm{j}2\pi Nf}\left(\mathbf{v}_{\text{re}}(f)^T\mathbf{p}_{\text{re}} + \mathbf{v}_{\text{im}}(f)^T\mathbf{p}_{\text{im}}\right), \tag{4}$$

where

$$\mathbf{v}_{\text{re}}(f) = [1, 2\cos(2\pi f), \ldots, 2\cos(2\pi Nf)]^T \tag{5}$$

$$\mathbf{v}_{\text{im}}(f) = [0, 2\sin(2\pi f), \ldots, 2\sin(2\pi Nf)]^T. \tag{6}$$

Applying the framework from [7], we then formulate the filter design optimization problem as the minimization of a squared error between the desired pulse spectrum mask $D(f)$ and actual pulse spectrum amplitude $P(f)$, i.e., we solve

$$\min_{\mathbf{p}_{\text{re}},\mathbf{p}_{\text{im}}} \int_{-F_{\text{s}}/2}^{F_{\text{s}}/2} \left(D(f) - \left|\mathbf{v}_{\text{re}}(f)^T\mathbf{p}_{\text{re}} + \mathbf{v}_{\text{im}}(f)^T\mathbf{p}_{\text{im}}\right|\right)^2 df \tag{7}$$

$$\text{subject to } \left|\mathbf{v}_{\text{re}}(f)^T\mathbf{p}_{\text{re}} + \mathbf{v}_{\text{im}}(f)^T\mathbf{p}_{\text{im}}\right| \le D(f), \quad \forall f \in [-F_{\text{s}}/2, F_{\text{s}}/2] \tag{8}$$

where F_{s} denotes the sampling frequency. The optimization problem becomes a convex quadratic problem through the discretization of the frequency axis and can efficiently be solved using interior point algorithms. The optimized pulse shape selected for the numerical results in Section IV is illustrated in Fig. 1. Relative to the center frequency, the amplitude frequency response of the custom pulse varies by ± 5 dB in its transmission band.

The receiver architecture for the multi-carrier sheme is shown in Fig. 3 (right subfigure). It is more similar to the receiver processing of a conventional microwave transmission system than that for the superposition scheme, as each data stream can be detected in parallel due to the negligible cross interference.

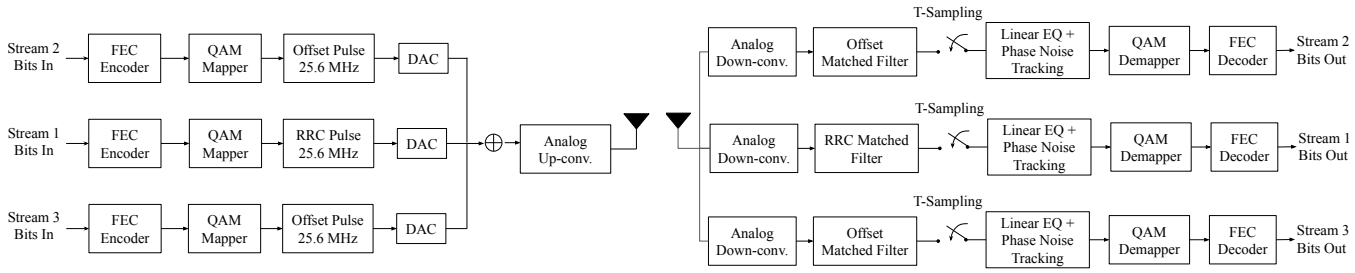

Fig. 3: Multi-Carrier transmission scheme architecture. The example of 25.6 MHz wide pulse shapes is illustrated at the transmitter side, consistent with the PSD for multi-carrier transmission shown in Fig. 1.

III. Channel Extrapolation

One challenge we encounter when demodulating the side-band signals in both modular schemes is obtaining a channel estimate required for equalization. While the primary stream in both modular schemes enjoys a high SNR and thus reliable channel estimation, this is not the case for the secondary streams, which are transmitted with a relatively lower power to fit under the spectrum skirts. This problem is particularly pronounced for the superposition transmission, where residual interference from the primary scheme limits the effective SNR experienced by the secondary stream.

To deal with this as well as to avoid extra pilot signal overhead for channel estimation for the secondary streams, we make use of the fact that the primary and secondary stream signals pass through the same channel, albeit with different bandwidths in the case of superposition transmission or in different frequency bands in the case of multi-carrier transmission. In particular, since the impulse-response representation of typical microwave channels typically allows for a description with very few parameters (see [6]), we can estimate those parameters from pilot signals in the primary stream and use the corresponding channel estimate for the secondary streams.

Considering a channel impulse response $h(t)$ with L significant taps, e.g. $L = 2$ for the commonly used Rummler channel model [6], and denoting the convolution of the transmitter RRC pulse and its receiver matched filter as $p'(t)$, we can express the overall impulse response as

$$c(t) = \sum_{l=1}^{L} c_l p'(t - t_l) \,, \tag{9}$$

where $\{t_l, c_l\}_{l=1}^{L}$ correspond to the unknown time delays and amplitudes of the transmission channel. The signal $c(t)$ fits the model of a signal with finite rate of innovation and we thus follow the methods from [8], [9] to estimate the desired parameters $\{t_l, c_l\}_{l=1}^{L}$. For this, we choose a T_c such that $c(t > T_c) \approx 0$ and write the Fourier series expression

$$c(t) = \sum_{k=-\infty}^{\infty} C[k] \mathrm{e}^{\mathrm{j}\frac{2\pi}{T_c}kt} \tag{10}$$

with the Fourier series coefficients

$$C[k] = \frac{1}{T_c} P'\left(\frac{2\pi}{T_c}k\right) \sum_{l=1}^{L} c_l \mathrm{e}^{-\mathrm{j}\frac{2\pi}{T_c}kt_l}, \tag{11}$$

where $P'(f)$ represents the continuous-time Fourier transform of $p'(t)$. Removing the effect from the pulse shapes and defining $z_l = \mathrm{e}^{-\mathrm{j}\frac{2\pi}{T_c}t_l}$, we get

$$X[k] = \frac{1}{T_c} \sum_{l=1}^{L} c_l \mathrm{e}^{-\mathrm{j}\frac{2\pi}{T_c}kt_l} = \frac{1}{T_c} \sum_{l=1}^{L} c_l z_l^k, \tag{12}$$

which is solely determined by the transmission channel. To obtain an estimate of z_l in (12), we apply the subspace method from [9], which is summarized in the following algorithm.

Algorithm: Subspace method for microwave channel estimation

1: Using $M + K - 1$ samples of $X[k]$, construct a $M \times K$ Hankel Matrix

$$\mathbf{X} = \begin{bmatrix} X[0] & X[1] & \cdots & X[K-1] \\ X[1] & X[2] & \cdots & X[K] \\ \vdots & & & \\ X[M-1] & X[M] & \cdots & X[M+K-2] \end{bmatrix}, \tag{13}$$

where $M, K > L$.

2: Compute the singular-value decomposition $\mathbf{X} = \mathbf{U}\mathbf{S}\mathbf{V}^H$.

3: Find the L largest singular values and the corresponding left singular vectors $\mathbf{U}_L$.

4: Compute estimates of $\hat{z}_l$ from (12) as the eigenvalues of the matrix $\underline{\mathbf{U}}_L^+ \cdot \bar{\mathbf{U}}_L$, where $(\cdot)^+$ represents the pseudo-inverse and the overbar and underbar symbols represent omitting the first and last row of $\mathbf{U}_L$, respectively.

Given $\hat{z}_l$ from the subspace method, we estimate the channel time delays as

$$t_l = \frac{T_c \angle \hat{z}_l}{2\pi}. \tag{14}$$

Finally, to obtain the channel coefficients, we transform (12) into a Vandermonde matrix

$$\mathbf{P} = \begin{bmatrix} 1 & \hat{z}_1 & \hat{z}_1^2 & \cdots & \hat{z}_1^{M+K-1} \\ \cdots & \cdots & & \cdots & \\ 1 & \hat{z}_L & \hat{z}_L^2 & \cdots & \hat{z}_L^{M+K-1} \end{bmatrix} \tag{15}$$

and solve the system of equations as

$$[\hat{c}_1 \ldots, \hat{c_L}] = [X[0], \ldots, X[M+K-2]]\mathbf{P}^{+} \, . \tag{16}$$

One modification we make to the original subspace algorithm is iterating over a number of choices for M to generate various matrices $\mathbf{X}$ (13). We then select a final set of $\{\hat{t}_l, \hat{c}_l\}_{l=1}^{L}$ coefficients that minimize the mean squared error between the estimated coefficients for the narrowband channel $c[k]$ using conventional pilot-based estimation, and a reconstruction of the narrowband channel $\hat{c}[k]$ using the subspace method.

IV. Simulations and Results

In this section, we demonstrate the benefits of the proposed transmission schemes through numerical results for achievable data rates and bit-error rate (BER) simulations. We adopt the dispersive Rummler channel model from [6] with a 5 dB notch and transmitter and receiver phase noise at an aggregate level of -90 dBc/Hz at an offset of 100 kHz, which is a significant yet typical phase noise level for microwave systems. We apply a linear minimum mean-square error (MMSE) equalizer to compensate for the Rummler transmission channel. We estimate and compensate the phase noise via the forward-backward algorithm described in [10] with pilots every 50 data symbols (see [3] for more details of the compensation methods). The signal pulse shapes and thus PSDs are set according to the spectrum mask shown in Fig. 1, where $1/T_1 = 25.6$ MHz, $1/T_2 = 51.2$ MHz and $1/T = 25.6$ MHz in (1) and (3), respectively. For the following, we show results as a function of the SNR defined as the symbol energy divided by the noise power per bandwidth unit (or PSD) of the baseline RRC-shaped transmission. This means we consider a scenario where the conventional RRC-based microwave system is operated at a certain SNR, and then the secondary data streams are being added by using the spectrum skirts.

First, Fig. 4 shows the BER results for the superposition and multi-carrier architectures. We use 2^{12} and 2^{14}-QAM for the primary streams of the superposition and multi-carrier schemes, respectively, and 2^m-QAM with $m = 2, 4$ for their secondary streams. A low-density parity-check (LDPC) code with rate 0.75 and codeword length 64800 bits is used for channel coding. We focus on the BER for the secondary streams in Fig. 4 to illustrate the effect of constellation size and phase noise. Considering the idealized case of transmission over a Rummler channel without phase noise first (dashed lines), we observe quite similar BER curves for the secondary streams with $m = 2$ for superposition and multi-carrier transmission. Increasing the modulation order to $m = 4$, i.e., 16QAM, we notice a significant SNR shift of the BER curves, which is due to the linear equalization which operates

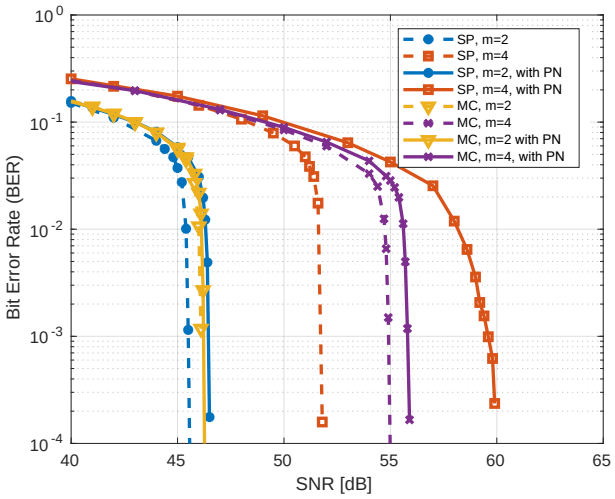

Fig. 4: BER for the secondary streams for: (1) Superposition (SP) transmission with 2^{12}-QAM for the primary data stream and 2^m-QAM for the secondary data stream; (2) multi-carrier transmission with 2^{14}-QAM for the primary data stream and 2^m-QAM for the two secondary streams. A Rummler channel without and with phase noise (PN) and FEC coding with a rate-0.75 LDPC code are considered.

at a low SNR for the secondary streams. If phase noise is present (solid lines), we notice the higher sensitivity of the superposition compared to the multi-carrier scheme. This is due to the imperfect interference cancelation of the main data stream as a result of residual phase noise.

Next, Fig. 5 shows the comparison between conventional RRC-based microwave transmission and the two proposed schemes in terms of the achievable information rate (AIR) [11], [12]. The AIR is measured empirically using the decision metrics (log-likelihood ratios) at the receiver, and we consider it as a practical estimate for the achievable rate with coded transmission [12]. The AIR curves in Fig. 5 correspond to the reference case of an AWGN channel (dashed lines) and the microwave transmission scenario of dispersive Rummler channel and phase noise (solid lines). The AIR is presented in terms of bits per RRC channel use, which translates into bits per second by multiplying it with the RRC baud rate of $1/T_1 = 25.6$ MHz. We observe a notable rate loss between the AWGN and microwave channel scenarios for all schemes. The main limiting factor for the performance of the latter is the phase noise. In particular, this prevents the use of constellations larger than 2^{14}-QAM for the conventional transmission systems. For example, the AIR curve for 2^{16}-QAM (not shown) falls below the one for 2^{14}-QAM in the microwave channel with phase noise. On the other hand, it can be seen that the proposed modular schemes, due to transmission of data in the spectrum skirts, yield significant rate gains over a wide range of practical SNRs for microwave links. For example, the data rate is improved by 28% to 38% at an SNR of 50 dB. We selected configurations for the primary and secondary data streams that demonstrated preferable performance, but further optimization, in particular

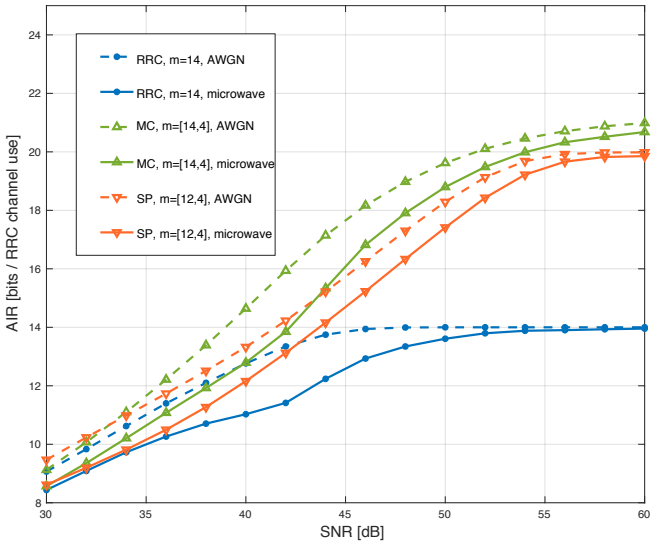

Fig. 5: AIR for different transmission systems: (1) conventional RRC-based transmission with 2^{14}-QAM; (2) multi-carrier (MC) transmission with 2^{14}-QAM in the primary data stream and 2^4-QAM in the two secondary data streams; (3) Superposition (SP) transmission with 2^{12}-QAM in the primary data stream and 2^4-QAM in the secondary data stream. AWGN channel and microwave channel (Rummler channel and phase noise) are considered. AIR is presented in terms of bits per RRC channel use.

adaption as a function of SNR, is possible. The multi-carrier scheme outperforms the superposition transmission, mainly due to the challenge of sufficiently accurate regeneration of the primary stream for interference cancellation in the latter method. Overall, we conclude that the modular spectrum utilization is highly beneficial to improve transmission rates in microwave links.

V. Conclusions

We have proposed the use of spectrum skirts for data transmission in microwave links by adding secondary data streams. The motivation for this approach is the frequent vacancy of adjacent frequency channels and the high operating SNR of microwave links, as well as the practical limitation for the use of higher-order modulations due to phase noise. In the superposition transmission scheme, the secondary data stream is added to the primary data stream, occupying a larger bandwidth and operating at very low power so as to respect the spectrum mask. In the multi-carrier transmission scheme, two side-band signals are added, with custom-made pulse-shapes and again very low power to fit under the mask. We have developed a channel estimation method for the proposed modular transmission systems that enables reliable detection of the sideband signals in relatively low SNR. Numerical results for practical channel and phase-noise scenarios indicate significant rate improvements of more than 30% at typical operating SNRs. These benefits are achieved without additional licensing costs and are complementary to gains obtained from other methods for improved spectral efficiency such as multi-antenna transmission.

References

[1] J. Saunders, "Mobile backhaul options - spectrum analysis and recommendations," GSM Association, ABI Research, GSMA Head Office, Floor 2, The Walbrook Building, 25 Walbrook, London EC4N 8AF, United Kingdom, Tech. Rep., September 2018. [Online]. Available: https://www.gsma.com/spectrum/wp-content/uploads/2019/04/Mobile-Backhaul-Options.pdf

[2] "Universal licensing system," https://wireless2.fcc.gov/UlsApp/UlsSearch/searchAdvanced.jsp, accessed: March 20, 2021.

[3] E. Dobre, A. Mostafa, L. Lampe, M. ShahMohammadian, and M. Jian, "Efficient spectrum utilization via pulse shape design for fixed transmission networks," *IEEE Trans. Commun.*, pp. 1510–1523, Mar. 2021.

[4] X. Huang, Y. J. Guo, A. Zhang, and V. Dyadyuk, "A multi-gigabit microwave backhaul," *IEEE Communications Magazine*, vol. 50, no. 3, pp. 122–129, 2012.

[5] ETSI, "Characteristics and requirements for point-to-point equipment and antennas; Part 2: Digital systems operating in frequency bands from 1.3 GHz to 86 GHz," Tech. Rep., Jun. 2016.

[6] W. Rummler, "More on the multipath fading channel model," *IEEE Trans. Commun.*, vol. 29, no. 3, pp. 346–352, Mar. 1981.

[7] T. N. Davidson, "Enriching the art of FIR filter design via convex optimization," *IEEE Signal Process. Mag.*, vol. 27, no. 3, pp. 89–101, May 2010.

[8] K. Gedalyahu, R. Tur, and Y. C. Eldar, "Sampling of pulse streams: Achieving the rate of innovation," in *IEEE Sensor Array and Multichannel Signal Processing Workshop*, Israel, 2010, pp. 133–136.

[9] I. Maravic and M. Vetterli, "Sampling and reconstruction of signals with finite rate of innovation in the presence of noise," *IEEE Trans. Signal Process.*, vol. 53, no. 8, pp. 2788–2901, Aug. 2005.

[10] H. S. Mohammadian and A. Aharony, "Accurate BCJR-based synchronization algorithm for single carrier channels with extremely high order modulations," in *International Conference on Signal Processing and Communication Systems (ICSPCS)*, Australia, 2016, pp. 1–6.

[11] D. M. Arnold, H.-A. Loeliger, P. O. Vontobel, A. Kavcic, and W. Zeng, "Simulation-based computation of information rates for channels with memory," *IEEE Trans. Inf. Theory*, vol. 52, no. 8, pp. 3498–3508, Aug. 2006.

[12] A. Alvarado, T. Fehenberger, B. Chen, and F. M. J. Willems, "Achievable information rates for fiber optics: Applications and computations," *J. Lightw. Technol.*, vol. 36, no. 2, pp. 424–439, Jan. 2018.